Saturation broadening by inhomogeneous fields

J. C. Camparo
The Aerospace Corporation, P.O. Box 92957, Los Angeles, California 90009
(Received 26 August 1988)

According to the standard Karplus-Schwinger theory of saturation broadening, saturated line shapes are Lorentzians with linewidths that increase linearly with the perturbing field strength. This, however, is not what is observed experimentally when the saturating field is inhomogeneous. If the saturating field strength varies significantly over the experimental signal volume, we find that the saturated line shapes are strikingly non-Lorentzian. The "sharpness" of the experimental line shapes is quantified by an "effective linewidth," which is the half width at half maximum of a Lorentzian that approximates the experimental line shape near line center. For certain classes of inhomogeneous fields, we find that this effective linewidth increases approximately as the square root of the saturating field strength, rather than linearly. We show that this class of inhomogeneous fields is distinguished by the presence of a node in the field geometry, and that the effect arises because the line shape near line center is dominated by the atomic population in the vicinity of the node. These results indicate the importance of understanding and accounting for inhomogeneous field effects when extracting physical information from experimental line shapes.

I. INTRODUCTION

In the mid to late 1940s Townes,[1] Karplus and Schwinger,[2] and Snyder and Richards[3] were concerned with the problem of collision broadening in the presence of intense electromagnetic radiation fields, and as a result initiated the study of saturation- (or power-) broadened resonance line shapes.[4] Working in the impact approximation for the collision process, Karplus and Schwinger showed that though resonance line shapes retain their Lorentzian character in the presence of strong fields, the width of the Lorentzian will be larger than that expected from relaxation alone. Defining $\Delta\nu$ as the resonance linewidth [half-width at half maximum (HWHM)], Karplus and Schwinger obtained a simple relationship between the linewidth and the field-atom interaction strength,

$$\Delta\nu=[\gamma^2+(\mu F/h)^2]^{1/2} . \quad (1)$$

Here μ is a transition matrix element, F is the field strength, and γ is the quantum system's relaxation (dephasing) rate.

As a consequence of the Lorentzian character of the Karplus-Schwinger line shape, the saturation-broadened linewidth provides a good measure of "line-shape sharpness," and hence a good estimate of the spectroscopic ability to find a saturated resonance's center frequency. Though the actual measure of line-shape sharpness is the line shape's second derivative evaluated at the resonance frequency, in the case of a Lorentzian it is quite easy to show that

$$\Delta\nu=\sqrt{-2S(\nu_0)/S''(\nu_0)} , \quad (2)$$

where $S(\nu_0)$ is the signal amplitude at the resonance frequency ν_0 and $S''(\nu_0)$ is the corresponding value of the second derivative. Thus, since saturation-broadened line shapes are expected to retain their Lorentzian character, the Karplus-Schwinger linewidth formula, Eq. (1), has the spectroscopic implication that in the saturation regime the ability to find a resonance's center frequency decreases inversely to the field strength (i.e., $\sqrt{S''(\nu_0)}\sim 1/F$).

In recent years some of the interest in saturation-broadened line shapes has been directed towards extending the theory of collision broadening in strong fields to situations where the impact approximation is not valid,[5,6] and experimentally verifying the Karplus-Schwinger linewidth formula in the optical regime.[7] There has also, however, been considerable interest in extending experimental research into regimes where the assumptions of the Karplus-Schwinger theory may be only marginally valid. For example, power broadening has been examined in regimes where the radiation field bandwidth is non-negligible.[8] Additionally, deviations from the Karplus-Schwinger linewidth formula have been observed in solids;[9] they have been observed when the dephasing rate $1/T_2$ is not equal to the longitudinal relaxation rate $1/T_1$;[10] and they have been observed when the quantum system has more than just two levels.[11]

A significant assumption in the Karplus-Schwinger theory is homogeneity of the field over the experimental signal volume. However, for the real fields employed in the laboratory this assumption is never rigorously satisfied. Hence, a question arises as to the shape of saturated resonances when this assumption is relaxed; specifically, when the field shows significant inhomogeneity over the signal volume. This question is of more than just academic interest, since the magnetic resonance signal of atomic clocks and masers is often stimulated by a specific microwave-cavity mode. In the present study we therefore relax the assumption of field homogeneity, and examine the resulting non-Lorentzian character of

saturation-broadened resonances.

In the following sections attention will focus on the spectroscopically important relationship between the average saturating field strength and line-shape sharpness. In Sec. II an experiment examining the saturated line shape of an atom confined in the inhomogeneous field of a microwave cavity will be described. As will be shown, the saturated line shapes obtained in this experiment differ markedly from the Lorentzian line shapes expected from the Karplus-Schwinger theory. Then in Sec. III the results from a numerical simulation of the experiment and its cavity mode field geometry will be presented and discussed, as well as simulations of experiments employing other types of field geometries. The results from these calculations will highlight those spatial properties of the field that have a primary influence on the shape of the saturated resonance. Finally, in Sec. IV, using the conclusions of the previous sections, we will present an approximate analytic solution to the problem of a saturated resonance's line shape. The purpose of this section will be to gain physical insight into why the saturated atomic resonance displays a non-Lorentzian shape.

II. EXPERIMENT

In order to examine saturation broadening in the presence of inhomogeneous electromagnetic fields, at least two conditions must be present in the experimental design. Obviously, it is necessary that the field exhibit sufficient inhomogeneity in order that the field's spatial variations are manifested in the observed line shape. Additionally, it is necessary that the atomic motion be "slow" so that the atoms do not motionally average the field inhomogeneities. Both of these conditions can be met in experiments examining the 0-0 hyperfine transition line shape in optically pumped alkali-metal vapors. Additionally, as a result of Dicke narrowing,[12] Doppler broadening does not confound the experimental results.

The experimental arrangement is shown schematically in Fig. 1. Light from a Mitsubishi ML-4102 single-mode diode laser,[13] tuned to the D_2 resonance of Rb at 780.2 nm, was allowed to pass through a ~ 1 cm orifice in the front face of a microwave cavity and into an atomic resonance cell. The total output power of the laser at the D_2 resonance was 2.5 mW, and it had a single-mode linewidth (full width at half-maximum) of 44 MHz. Additionally, in an attempt to probe atoms throughout the cavity volume, the beam was made to diverge after passing through a lens; a beam diffusing element was placed over the cavity orifice, and a photodiode for detecting the transmitted light was placed inside the cavity. (The sensitive area of the photodiode was approximately equal to the cross-sectional area of the cavity.) By centering the cavity and resonance cell in a pair of Helmholtz coils, which produced an axial static magnetic field of several gauss, the ground-state Zeeman degeneracy was lifted so that only the $(m_F=0)$-$(m_F=0)$ hyperfine transition was resonant with the cavity's microwave field.

A vapor of natural Rb (28% ^{87}Rb and 72% ^{85}Rb) in equilibrium with a droplet of liquid metal at approximately 64 °C was contained in a cylindrical Pyrex resonance cell along with 100 torr of N_2. The nitrogen was present in order to both reduce the contribution of wall collisions to the atomic systems's relaxation rate,[14] and to limit motional averaging of the field. The resonance cell was placed inside a microwave cavity whose TE_{111} mode was resonant with the ^{87}Rb 0-0 ground-state hyperfine transition. The spatial variation of the TE_{111} mode's axial magnetic field component, which is the field component responsible for exciting the 0-0 transition, is given by[15]

$$F_z(r,\phi,z)=F_0 J_1(1.841r/R)\cos(\phi)\sin(\pi z/L)\ , \tag{3}$$

where $J_1(x)$ is a first-order Bessel function, R is the cavity radius, and L its length; the radial and angular variations of this field mode are illustrated in Fig. 2. This particular cavity mode was chosen because the field geometry has a nodal plane, which is a condition of significant field inhomogeneity. As a result of the high nitrogen density motional averaging of the field inhomogeneity was negligible. Under the experimental conditions the atomic diffusion coefficient D had the value 1.4 cm^2/sec,[16] so that the rms atomic spatial displacement $\delta 1$

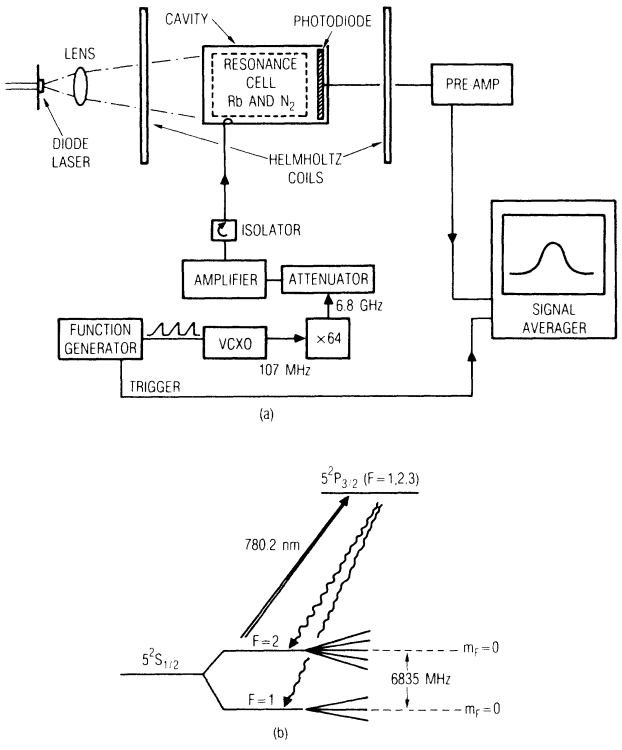

FIG. 1. (a) shows the experimental arrangement. A diode laser optically pumps ^{87}Rb atoms contained in a Pyrex glass resonance cell. The resonance cell is located inside a microwave cavity whose TE_{111} mode is resonant with the alkali-metal-atom's ground-state 0-0 hyperfine transition. The microwaves are supplied to the cavity through the chain of rf multiplication and amplification shown in the figure. (b) illustrates the pertinent energy levels of ^{87}Rb. Depopulation optical pumping creates a population imbalance (i.e., hyperfine polarization) between the alkali-metal ground-state hyperfine manifolds, which is perturbed by the strong microwave field at ~ 6835 MHz.

was estimated as 0.17 cm (assuming a 10 msec dephasing time T_2 and taking $\delta l = \sqrt{2DT_2}$); this is to be compared with the microwave cavity's 2.7 cm diameter and 3.8 cm length.

Microwave power was supplied to the cavity through the chain of rf multiplication and amplification shown in Fig. 1(a). Since the power entering the cavity is proportional to the stored energy in the cavity,[15] the attenuators placed in the microwave path could be used to vary the magnitude of the average field strength in a well defined manner. Additionally, the frequency of the approximately 106.8 MHz rf coming from the voltage-controlled oscillator was ramped by a function generator, so that the microwave frequency swept slowly over the 0-0 hyperfine transition.

By tuning the diode laser to the D_2 ^{87}Rb transition $[5\,^2P_{3/2}(F=1,2,3)-5\,^2S_{1/2}(F=2)]$ the atomic population in the $F=2$ ground-state hyperfine manifold was transferred by depopulation optical pumping into the $F=1$ ground-state hyperfine manifold.[14] In the absence of microwaves at the appropriate frequency, this resulted in a maximum for the light intensity transmitted through the resonance cell. As the microwaves swept over the 0-0 hyperfine transition at 6835 MHz, atoms in the ($F=1$, $m_F=0$) Zeeman sublevel returned to the ($F=2$, $m_F=0$) Zeeman sublevel, with the effect of reducing the transmitted laser intensity. Since the atoms were locally confined by the nitrogen buffer gas, the change in transmitted light intensity associated with any particular region of the vapor depended upon the local field strength in that region, and the region's initial (equilibrium) population imbalance due to optical pumping. The observed change in transmitted laser intensity thus mapped out the full signal volume's 0-0 hyperfine transition line shape as the microwave frequency was scanned across the hyperfine resonance, and this line shape was recorded with a signal averager.

An example of a saturated line shape obtained in this experiment is shown in Fig. 3(a). Since the intrinsic HWHM of the transition under the experimental conditions was ~ 1 kHz, the observed ~ 25 KHz HWHM for this experimental line shape implies a condition of extreme saturation broadening. For comparative purposes the figure also shows a Lorentzian line shape with the same HWHM as the experimental line shape, and it is clear even visually that the experimental line shape deviates significantly from a Lorentzian. Specifically, the experimental line shape appears to be sharper than a Lorentzian of the same linewidth. In order to quantify the relative sharpness of the observed saturated resonances, we define an "effective linewidth" $\delta\nu$ which is re-

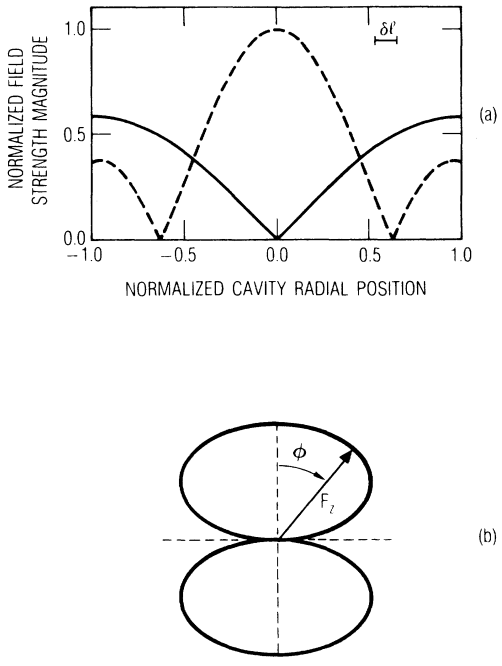

FIG. 2. This figure illustrates various spatial variations of the microwave magnetic field's axial component (F_z); it is this component of the electromagnetic field which is responsible for the transitions between the $m_F=0$ Zeeman sublevels of the alkali-metal ground state. In (a) the radial variation of $|F_z|$ is shown for both a TE_{111} cavity mode (solid line) and a TE_{011} cavity mode (dashed line). For illustrative purposes the relative rms atomic spatial displacement δl discussed in the text is also shown. (b) is a polar plot showing the variation of F_z with azimuthal angle ϕ for a TE_{111} cavity mode; the TE_{011} mode has azimuthal symmetry, so there is no ϕ dependence.

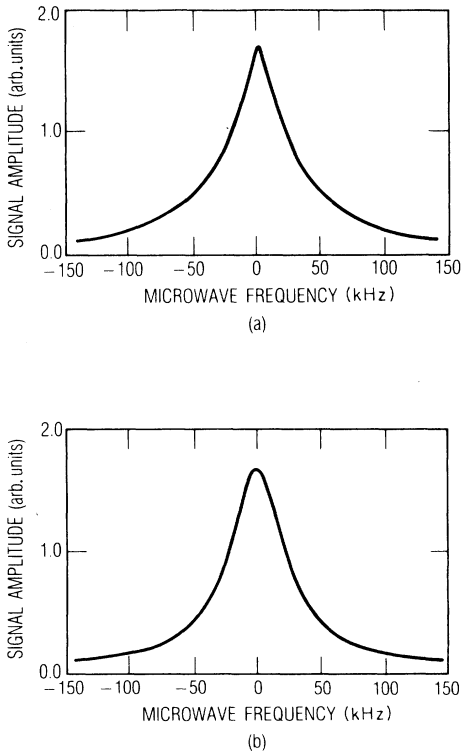

FIG. 3. (a) shows the experimental saturated line shape obtained from the TE_{111} mode field geometry. (b) is a Lorentzian line shape of the same half-width half-maximum (HWHM). It is clear that the saturated line shapes obtained with the inhomogeneous field differ significantly from the Lorentzians predicted by the Karplus-Schwinger theory.

lated to the resonance line shape's second derivative through Eq. (2) [$S''(\nu_0)$ was obtained from the line-shape data stored in the signal averager by numerical differentation]. In essence $\delta\nu$ is the linewidth of the Lorentzian that approximates the experimental line shape near line center, so that in regimes where the Karplus-Schwinger theory is valid, one would have $\Delta\nu=\delta\nu$.

The results of this analysis are shown in Fig. 4, where the effective linewidth ($\delta\nu$) and the HWHM ($\Delta\nu$) are plotted as a function of the average field strength in the microwave cavity. The straight lines represent least-squares fits to the data, assuming a power-law scaling relation between linewidth and field strength

$$\Delta\nu \sim \langle F \rangle^{\alpha} \tag{4a}$$

and

$$\delta\nu \sim \langle F \rangle^{\beta} . \tag{4b}$$

Since a power-law relation should only be valid when the intrinsic width of the saturated resonance is negligible, the lowest field strength data were excluded from the analysis (since the intrinsic linewidth must be less than or equal to this value).

The data of Fig. 4 support the previous qualitative conclusion that the observed line shape is sharper than a Lorentzian of the same half-width. This is illustrated in Fig. 4 by the fact that the effective linewidth is always smaller than the HWHM. Additionally, the data show that the HWHM and the effective linewidth increase at different rates as the magnitude of the average field strength increases. As evidenced by the values of α and β given in the figure, it appears that the HWHM increases in a nearly linear fashion with the field strength ($\alpha\sim 1$), consistent with the Karplus-Schwinger theory, while the effective linewidth exhibits a square-root dependence on field strength magnitude ($\beta\sim\frac{1}{2}$).

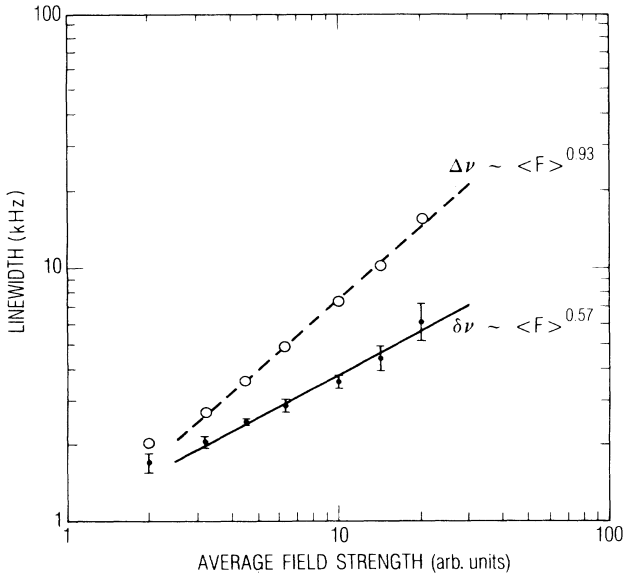

FIG. 4. Plot of the experimental HWHM ($\Delta\nu$) and effective linewidth ($\delta\nu$) vs average field strength $\langle F \rangle$. The data were fit to power-law scaling relations to determine the values of the exponents shown in the figure.

Naively, these results might be taken as strong evidence that field inhomogeneity has a pronounced effect on the saturation-broadening behavior of experimental line shapes. However, it is important to mention that the high nitrogen density used in this experiment has a further consequence for the observed line shape. It is well known that as a result of the strongly relaxing glass surface, the presence of a buffer gas results in spatial modes for the population imbalance between the two hyperfine manifolds.[17] Consequently, not all spatial regions within the field contribute to the observed line shape to the same degree. Hence, the experimentally observed line shape is a manifestation of *two* inhomogeneities: one due to the field, and the other due to the equilibrium population imbalance (i.e., the population imbalance between the two states in the absence of the microwave field). At this point in the discussion we can only suggest that the observed saturation-broadening behavior is associated with the field's inhomogeneity. In the next section we will address this problem with a series of numerical simulations of the experiment. Our method will be to unravel the various spatial variations that might give rise to this behavior, and to see separately the effect of each on the macroscopic line shape.

III. NUMERICAL SIMULATION

The numerical simulation of the preceding 0-0 hyperfine transition line-shape experiment has been extensively discussed in previous publications.[18–21] Therefore, only a brief description of the simulation, highlighting some of its salient features, will be given here. In the calculations the relevant gas-phase physics occurs on two different scales. On the microscopic scale, the line shape is determined by the generalized Vanier theory.[11] This density-matrix theory describes the multi-Zeeman level optical pumping process which results in the alkali-metal hyperfine polarization (i.e., the population imbalance between the two hyperfine manifolds), and yields a Lorentzian 0-0 hyperfine transition line shape, with a HWHM that depends on the field strength in a fashion analogous to Eq. (1).[22] However, since atoms in different regions of the cavity experience different microwave-field strengths, and since atomic diffusion through the molecular buffer gas yields spatial modes of hyperfine polarization,[17] the microscopic response to the field varies on the macroscopic scale of the field's and polarization's spatial distributions.

In practice the observed (macroscopic) line shape is calculated by dividing the cylindrical cavity volume into thousands of small tubes, minimally 4300, and calculating the total optical power transmitted by these tubes as a function of microwave frequency. The tubes are chosen to have a small diameter so that variations of field strength and hyperfine polarization across the tube face are not appreciable. Thus, for an individual tube the only spatial variation in either the field or the hyperfine polarization is an axial one. Each tube is associated with an appropriately normalized field strength value, so that any

particular transverse geometry for the field may be considered in the calculations. To account for the transverse spatial distribution of hyperfine polarization, an appropriate weighting function is superimposed onto the generalized Vanier theory solutions for each tube. For a given microwave detuning from resonance, and a given microwave field energy in the cavity, the optical power transmitted through each tube is determined by assuming a Bouger-Beer-Lambert law for optical attenuation: $I \sim I_0 \exp(-[N]\sigma L)$.[23] Here, $[N]$ is the average number density of absorbers in the tube of length L, which is a function of the axial distribution of microwave-field strength and hyperfine polarization. The optical powers transmitted by the tubes are then summed, which yields the observed signal amplitude for the specific microwave frequency detuning from resonance.

Considering the cases of a TE_{111} cavity mode, and using other parameters appropriate to the previously described experiment, Fig. 5 provides several examples of calculated line shapes for differing values of the average cavity mode field strength $\langle F \rangle$. (Nearly all the parameters required by the numerical simulation are measured; the only free parameters in the calculations are the microwave power entering the cavity and the cavity Q.) It is clear that as the average field strength increases, the HWHM increases, as observed experimentally. Additionally, for increasing values of $\langle F \rangle$ the line shapes display a growing deviation from the Karplus-Schwinger Lorentzian character. In particular, at the very highest value of $\langle F \rangle$ the resonance has a cusplike appearance, implying that the second derivative of this line shape is comparatively large given its HWHM (i.e., $\delta\nu \ll \Delta\nu$).

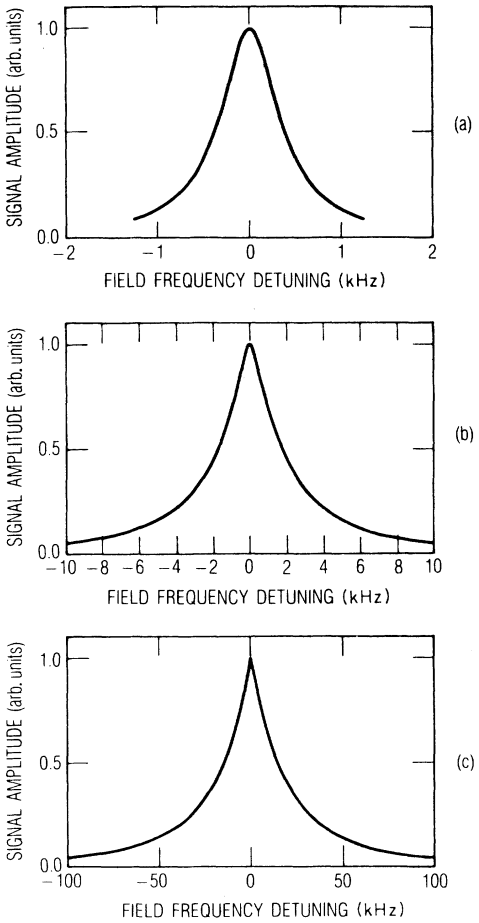

FIG. 5. Theoretical line shapes for three different values of the microwave power supplied to a TE_{111} cavity mode (cavity Q was set equal to 100): (a) microwave power is 0.001 mW, (b) microwave power is 0.1 mW, and (c) microwave power is 10.0 mW. Since the average field strength in the cavity is proportional to the square root of the power. (a)–(c) represent a factor of 100 change in the average field strength. Note that as the average field strength increases, the line shapes exhibit an increasing deviation from a Lorentzian shape.

To quantify the growing non-Lorentzian character of the saturated resonances, Fig. 6 shows the calculated HWHM and effective linewidth as a function of average field strength. The solid lines correspond to least-squares fits of the numerical data, and give exponents for the power-law scaling relations. Comparing Figs. 4 and 6 it is clear that there is reasonably good agreement between theory and experiment. In particular, the theoretical HWHM shows a nearly linear dependence on field strength, while the effective linewidth shows an approximately square-root dependence on field strength.

These theoretical results indicate that the source of the line-shape's non-Lorentzian character is properly modeled by some portion of the numerical simulation. Therefore, by examining the simulation's predictions under alternate "fictitious" conditions, where the various spatial distributions are eliminated one by one, it should be possible to uncover this portion of the numerical simulation, and hence the source of the observed line shape behavior. With this as a goal, several sets of calculations

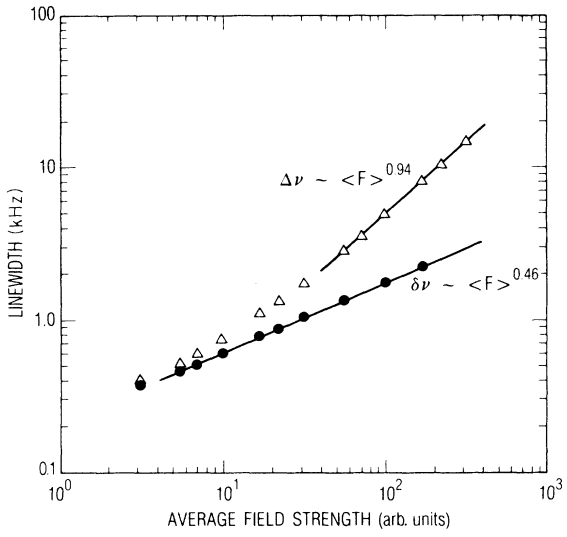

FIG. 6. Plot of the theoretical HWHM ($\Delta\nu$) and effective linewidth ($\delta\nu$) vs the average field strength $\langle F \rangle$. The calculation is for the specific case of a TE_{111} mode field geometry, as was used in the experiment. The numerical data were fit to power-law scaling relations to determine the values of the exponents shown in the figure.

were thus performed. In the first set we considered the same experiment, except that the axial field component of the TE_{111} mode was only allowed to exhibit an angular and axial spatial variation [i.e., we removed the radial dependence of the field from the calculations so that $F_z(r,\phi,z)\rightarrow F_z(\phi,z)$]. Similarly, in the second set we only allowed the field of the TE_{111} mode to vary along its radial and axial dimensions [i.e., we removed the angular dependence of the field from the calculations so that $F_z(r,\phi,z)\rightarrow F_z(r,z)$]. Then in the third set we removed both the radial and angular field variations from the calculations, so that the field of the TE_{111} mode had only an axial spatial variation [i.e., $F_z(r,\phi,z)\rightarrow F_z(z)$]. In all of the calculations the spatial distribution of hyperfine polarization was the same as that used in the previous TE_{111} mode simulation of the experiment.

The power-law exponents obtained from these fictitous simulations are collected in Table I, while Fig. 7 shows both $\delta\nu$ and $\Delta\nu$ as a function of average field strength for the $F_z(\phi,z)$ and $F_z(z)$ calculations. The dashed-dotted line and circles correspond to calculations of $\Delta\nu$ and $\delta\nu$, respectively, for the $F_z(z)$ calculations, while the dashed line and triangles correspond to $F_z(\phi,z)$ calculations of $\Delta\nu$ and $\delta\nu$, respectively. From Table I it is clear that the square-root dependence of $\delta\nu$ on field strength is a consequence of field inhomogeneity: as the field becomes homogeneous in the simulations, β approaches unity. Additionally, the simulations indicate that the $\frac{1}{2}$ value of β is primarily associated with the radial and angular field variations, and also that the $\frac{1}{2}$ value of β is more tightly coupled to the angular field variations than to the radial field variations (i.e., in the simulation where the radial field variations are removed β only increases by 0.04, but when the angular field variations are removed β increases by 0.17). Given that a field node implies a strong degree of field inhomogeneity, these observations are consistent with the hypothesis that the source of the saturated line shape's non-Lorentzian character is somehow associated with nodes in the field distribution.

With this hypothesis one would argue that the angular field variation is particularly important in determining the value of β, since this spatial variation yields a nodal plane for the field. The radial field variation might be viewed as somewhat less important, since it only results in a nodal field line. Both transverse variations could, however, be expected to yield significant departures from

TABLE I. Linewidth power-law exponents for different saturating electromagnetic field geometries: $\Delta\nu\sim\langle F\rangle^{\alpha}$, $\delta\nu\sim\langle F\rangle^{\beta}$. In the calculations the field was allowed to vary over the given spatial dimensions.

Condition	α	β
Experiment	0.93	0.57
TE_{111} mode calculation: $F_z(r,\phi,z)$	0.94	0.46
TE_{111} mode calculation: $F_z(\phi,z)$	0.90	0.50
TE_{111} mode calculation: $F_z(r,z)$	0.89	0.63
TE_{111} mode calculation: $F_z(z)$	0.98	0.84
TE_{011} mode calculation: $F_z(r,z)$	0.80	0.45
Analytic analysis		0.50

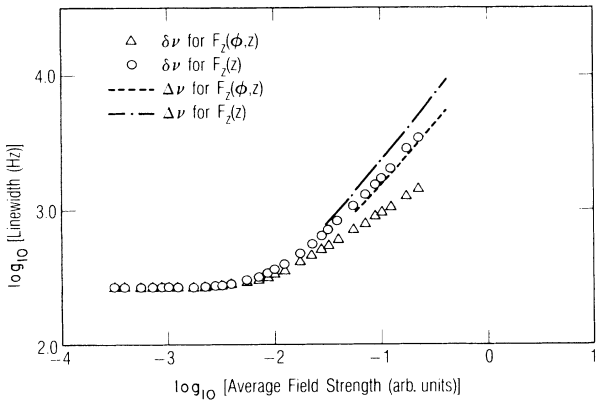

FIG. 7. Plot of the theoretical HWHM ($\Delta\nu$) and effective linewidth ($\delta\nu$) vs the average field strength $\langle F\rangle$. The dotted-dashed line and circles correspond to $\Delta\nu$ and $\delta\nu$ calculations, respectively, for the fictitious TE_{111} $F_z(z)$ mode; the dashed line and triangles correspond, respectively, to $\Delta\nu$ and $\delta\nu$ calculations for the fictitious TE_{111} $F_z(\phi,z)$ mode. The numerical data were fit to power-law scaling relations to determine the values of the exponents given in Table I.

the predictions of the Karplus-Schwinger theory. Alternatively, since the field nodes arising from the axial variations occur at the cavity boundaries, where no resonance signal is generated due to the strongly relaxing wall collisions, one would not expect axial variations to significantly alter the $\beta=1$ prediction of the Karplus-Schwinger theory.

If this conjecture on the role of field nodes is correct, it should be possible to make qualitative predictions on the value of β for field geometries other than the TE_{111} mode. Consequently, in our final numerical simulation we considered a field geometry corresponding to a TE_{011} cavity mode, which differs in basically two ways from the TE_{111} cavity mode: (i) as shown in Fig. 2(a) the radial nodes of the TE_{011} mode (axial field component) are at $r>0$, so that there is a nodal surface in the cavity due to the radial field distribution; and (ii) the axial field component of the TE_{011} mode has azimuthal symmetry. For both cavity modes, however, the axial field components exhibit the same axial variation of $\sin(\pi z/L)$. If the field node conjecture were true, one would expect to obtain a value of β from the simulation roughly equal to 0.5, and as recorded in Table I this was indeed the case. The numerical simulations thus strongly suggest that field nodes somehow lead to significant deviations from the Karplus-Schwinger theory of saturation broadening, and in the next section the specific role of field nodes in this regard will be addressed.

IV. ANALYTIC APPROXIMATION

In order to gain physical insight into the behavior of $\delta\nu$, which is the quantity of spectroscopic importance, we will consider in this section the one-dimensional problem of an ensemble of two-level atoms interacting with an inhomogeneous saturating electromagnetic field as illustrated in Fig. 8. We assume that the spatial motion of the atoms is "slow," so that during a time interval on the or-

der of the atom's dephasing time, the atom interacts with the strong field only in some small localized region. Thus, the signal as a function of field frequency is just the integral of the one-dimensional signal density $s(\nu,x)$:

$$S(\nu)=2\int_0^X s(\nu,x)dx \ . \tag{5}$$

Additionally, we will allow the equilibrium population difference between the two levels $(N_1^e-N_2^e)$ (i.e., the population difference between the two levels in the absence of any field) to be a function of position. Thus, taking the observed signal to be proportional to the increased population in the excited state, and assuming that on the local (microscopic) level the Karplus-Schwinger theory is appropriate for describing the strong-field interaction of the atoms, we have

$$S(\nu)=2\int_0^X \frac{\Delta n(x)\omega_1^2(x)}{[\gamma^2+\omega_1^2(x)+(\nu-\nu_0)^2]}dx \ , \tag{6a}$$

$$\Delta n(x)=n_1^e(x)-n_2^e(x) \ , \tag{6b}$$

where $n_i^e(x)$ is the equilibrium population density in the i^{th} state at the position x; $\omega_1(x)$ is the Rabi frequency at the position x, which specifies the local strength of the field-atom interaction $[\omega_1(x)=\mu F(x)/h]$, and ν_0 is taken

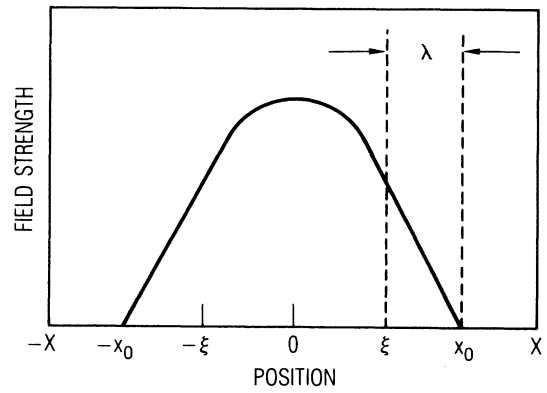

(a)

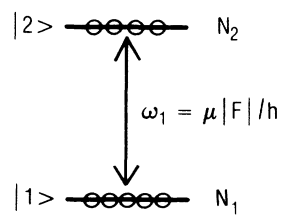

(b)

FIG. 8. (a) One-dimensional field geometry used in the analytic analysis of saturation broadening by inhomogeneous fields. The quantities x_0, ξ, and λ are described in the text. (b) Energy-level diagram of the simple two-level quantum system used in the analytic analysis.

to be independent of x (no inhomogeneous broadening[24]). It is clear that given the form of Eq. (6a), saturated resonances with Lorentzian line shapes need not be observed experimentally, except under very special circumstances. Consequently, in order to characterize line shape sharpness we again employ the effective linewidth $\delta\nu$ which is related to the resonance line shape's second derivative through Eq. (2).

Rewriting and differentiating Eq. (6a) with respect to frequency we find that

$$S(\nu_0)=2\int_0^X \Delta n(x)\omega_1^2(x)/[\gamma^2+\omega_1^2(x)]dx \ , \tag{7a}$$

and

$$S''(\nu_0)=-4\int_0^X \Delta n(x)\omega_1^2(x)/[\gamma^2+\omega_1^2(x)]^2dx \ . \tag{7b}$$

Note that if the Rabi frequency is independent of x, then

$$\delta\nu=(\gamma^2+\omega_1^2)^{1/2}=\Delta\nu \ , \tag{8}$$

and the effective linewidth increases in proportion to the field strength (when $\omega_1 \gg \gamma$) as expected for a homogeneous field. In the case where the Rabi frequency is not constant, however, the functional relationship between $\delta\nu$ and field strength is much less transparent.

To obtain such a relationship the first task is to compute $S(\nu_0)$, and we begin by defining the ensemble average equilibrium population difference between the two atomic states,

$$\langle \Delta N \rangle = \int_0^X \Delta n(x)dx \ . \tag{9}$$

One then finds that

$$S(\nu_0)=2\langle \Delta N \rangle - 2\gamma^2\int_0^X \Delta n(x)/[\gamma^2+\omega_1^2(x)]dx \ . \tag{10}$$

We next define a position $x_0-\lambda=\xi$ in the field such that the Rabi frequency at this position equals the atomic relaxation rate [i.e., $\omega_1(x=\xi)=\gamma$]. In this way we have the general conditions that

$$\text{if } |x|<|\xi| \text{ then } \omega_1(x)/\gamma>1$$

and

$$\text{if } |x|>|\xi| \text{ then } \omega_1(x)/\gamma<1 \ .$$

Splitting the integral of Eq. (10) into two parts, corresponding to the two different spatial regions defined above, we have

$$S(\nu_0)=2\langle \Delta N \rangle - 2\gamma^2\int_0^{\xi} \Delta n(x)/[\gamma^2+\omega_1^2(x)]dx - 2\gamma^2\int_{\xi}^X \Delta n(x)/[\gamma^2+\omega_1^2(x)]dx \ . \tag{11}$$

Here, the first integral accounts for the signal generated in the saturated spatial region of the ensemble, and the second integral accounts for the signal generated in the unsaturated region. Note that the first integral contains terms of order $[\gamma/\omega_1(x)]^2$ or higher, so that the magnitude of this term will be dominated by the spatial region where $\omega_1 \sim \gamma$. If the spatial extent of this region is relatively small, then the first integral makes a negligible contribution to the signal amplitude, and we have

$$S(\nu_0)\simeq 2\langle \Delta N\rangle - 2\gamma^2\int_{\xi}^{X}\Delta n(x)/[\gamma^2+\omega_1^2(x)]dx \ . \quad (12)$$

Physically, Eq. (12) indicates that the shape of the saturated resonance near line center is dominated by the unsaturated spatial regions of the ensemble.

We can narrow the limits of integration in Eq. (12) further by noting that for $x > x_0$ the Rabi frequency is zero. Thus, by defining a term Λ,

$$\Lambda \equiv \langle \Delta N\rangle - \int_{x_0}^{X}\Delta n(x)dx \ , \quad (13)$$

we have finally

$$S(\nu_0)\simeq 2\Lambda - 2\gamma^2\int_{\xi}^{x_0}\Delta n(x)/[\gamma^2+\omega_1^2(x)]dx \ . \quad (14)$$

To proceed further, we write the Rabi frequency as the product of the average field strength $\langle F\rangle$ and a function describing the spatial distribution of the field $f(x)$:

$$\omega_1(x)=(\mu/h)\langle F\rangle f(x) \ , \quad (15a)$$

$$\int_0^X f(x)\,dx/X = 1 \ . \quad (15b)$$

Expanding $\omega_1(x)$ in a Taylor series about x_0 we then have

$$\omega_1(x)=(\mu/h)\langle F\rangle[f(x_0)+(x-x_0)f'(x_0)+\cdots] \ . \quad (16)$$

For the case where x_0 corresponds to a node in the field strength distribution, as in the case considered here,

$$\omega_1(x)\simeq(\mu/h)\langle F\rangle(x-x_0)\eta \ , \quad (17)$$

and as a consequence

$$\lambda \simeq -h\gamma/(\mu\langle F\rangle\eta) \ , \quad (18)$$

where $\eta \equiv f'(x_0)$ (evaluated in the case of Fig. 8 from the direction of increasing $|x|$). The value of λ (i.e., the spatial extent of the unsaturated signal region), and hence the range of integration in Eq. (14), is thus found to be a monotonically decreasing function of the average field strength. Physically this corresponds to the fact that as the field strength increases, the unsaturated spatial region of the ensemble decreases in size. It is this phenomena that has important consequences for the shape of saturated resonances when the saturating field is inhomogeneous.

If we now assume that $\Delta n(x)$ is a slowly varying function of position over the range $\xi < x < x_0$, then we can replace $\Delta n(x)$ by its value at x_0. The resulting integral is easily evaluated, and we find that

$$S(\nu_0)\simeq 2\Lambda - \pi h\gamma\Delta n(x_0)/2\mu\langle F\rangle\eta \ . \quad (19)$$

The evaluation of $S''(\nu_0)$ proceeds along very similar lines, yielding

$$S''(\nu_0)\simeq -(3\pi+2)h\Delta n(x_0)/2\mu\langle F\rangle\eta\gamma \ . \quad (20)$$

Thus, using Eqs. (19) and (20) in Eq. (2) we obtain the effective linewidth $\delta\nu$ in the case of an inhomogeneous saturating field,

$$\delta\nu\simeq\sqrt{2\gamma/(3\pi+2)}[4\Lambda\mu\langle F\rangle\eta/h\Delta n(x_0)-\pi\gamma]^{1/2} \ , \quad (21)$$

which yields in the limit of very strong fields

$$\delta\nu\sim\langle F\rangle^{0.5} \ . \quad (22)$$

This result is exactly the line-shape behavior that we were attempting to explain. From the above derivation it is now clear that deviations from the Karplus-Schwinger prediction of $\beta=1$ arise because the line shape near line center is dominated by the unsaturated atomic population, and because the spatial region containing this population shrinks in size as the average field strength increases. With regard to $\Delta\nu$, since the above derivation suggests that *saturated* atomic population contributes primarily to the wings of the line shape, one would expect $\alpha > 0.5$.

V. SUMMARY

In this paper we have examined the line shape of saturated resonances when the atoms cannot motionally average an inhomogeneity that may be present in the saturating field. The results of this study show that under these conditions the saturated line shape is non-Lorentzian, and that the central portion of the resonance is primarily determined by those spatial regions of the field where the atoms are not yet saturated. Consequently, the observed resonance line shape is sharper than would be expected from the Karplus-Schwinger theory. By defining an effective linewidth $\delta\nu$, which is the linewidth of a Lorentzian that approximates the central portion of the resonance, the line shape's sharpness can be quantified and examined as a function of saturating field strength (i.e., $\delta\nu\sim\langle F\rangle^{\beta}$). For the specific case of nodes in the field's spatial distribution, we find that $\beta\sim 0.5$, as opposed to $\beta=1.0$ which is the value expected from the Karplus-Schwinger theory.

These results have important consequences for precision spectroscopy, especially in the area of atomic clocks where atomic signals are generated throughout the volume of some microwave cavity. Since the ability to find resonance line center can be quantified by a parameter which is inversely proportional to the effective linewidth,[25] the above results suggest that precision spectroscopy may not be as adversely affected by high intensity, inhomogeneous fields as one might expect given the Karplus-Schwinger theory (i.e., for an inhomogeneous field with a node, $\sqrt{S''(\nu_0)}\sim 1/\sqrt{F}$). For example, with a homogeneous field the Karplus-Schwinger theory predicts that an increase in radiation intensity (i.e., field energy) of 100 results in a factor of 10 loss in the ability to find resonance line center; however, if an inhomogeneous field has a node in its spatial distribution, then a 10^4 increase in radiation intensity is required in order to degrade this spectroscopic ability by the same factor of 10. (Of course in this simple example we have ignored the question of ac Stark and Bloch-Siegert shifts, which is an entirely different aspect of the inhomogeneous-field problem in spectroscopy.[24])

In one sense then, the above results indicate a further important restriction on the validity of the Karplus-Schwinger theory of saturation broadening. Regarded in a broader context through, the above results can be seen as an example of a class of phenomena that arises when one studies the field-atom interaction with real fields.

Real fields are never perfectly homogeneous, and the inhomogeneity can have important consequences for the outcome of many field-atom interaction experiments. In this regard it is worth noting that spatial field variations can play an important role in photoionization experiments, and caution must be exercised in the evaluation of multiphoton ionization cross sections in the absence of field inhomogeneity information.[26,27] In this broader context the present results similarly indicate how microscopic field-atom interactions are not always simply reflected in macroscopic experimental line shapes, when field inhomogeneities are present.

ACKNOWLEDGMENTS

The author would like to thank Dr. R. Frueholz and Dr. B. Jaduszliwer for critical readings of the manuscript, and Spencer Delcamp for help in performing the experiments. This work was supported by the U.S. Air Force Space Division under Contract No. F04701-86-C-0087.

[1]C. H. Townes, Phys. Rev. **70**, 665 (1946).
[2]R. Karplus and J. Schwinger, Phys. Rev. **73**, 1020 (1948).
[3]H. S. Snyder and P. I. Richards, Phys. Rev. **73**, 1178 (1948).
[4]It should be noted that it is often important to introduce a distinction between power and saturation broadening. For a discussion of these distinctions, see, for example, R. A. Van Calcar, M. J. G. Heuts, B. K. Van Uitert, H. A. J. Meijer, T. J. Hollander, and C. Th. J. Alkemade, J. Quant. Spectrosc. Radiat. Transfer **28**, 1 (1982).
[5]V. S. Lisitsa and S. I. Yakovlenko, Zh. Eksp. Teor. Fiz. **68**, 479 (1975) [Sov. Phys.—JETP **41**, 233 (1975)].
[6]Y. Rabin, D. Grimbert, and S. Mukamel, Phys. Rev. A **26**, 271 (1982).
[7]M. L. Citron, H. R. Gray, C. W. Gabel, and C. R. Stroud, Phys. Rev. A **16**, 1507 (1977).
[8]A. R. D. van Bergen, T. J. Hollander, and C. Th. J. Alkemade, J. Quant. Spectrosc. Radiat. Transfer **33**, 419 (1985).
[9]T. Endo, T. Muramoto, and T. Hashi, Opt. Commun. **51**, 163 (1984).
[10]N. D. Bhaskar, J. Camparo, W. Happer, and A. Sharma, Phys. Rev. A **23**, 3048 (1981).
[11]J. C. Camparo and R. P. Frueholz, Phys. Rev. A **31**, 1440 (1985); **32**, 1888 (1985).
[12]R. H. Dicke, Phys. Rev. **89**, 472 (1953); R. P. Frueholz and C. H. Volk, J. Phys. B **18**, 4055 (1985).
[13]J. C. Camparo, Contemp. Phys. **26**, 443 (1985).
[14]W. Happer, Rev. Mod. Phys. **44**, 169 (1972).
[15]J. D. Jackson, *Classical Electrodynamics* (Wiley, New York, 1975), pp. 356–360.
[16]F. A. Franz ad C. Volk, Phys. Rev. A **14**, 1711 (1976).
[17]P. Minguzzi, F. Strumia, and P. Violino, Nuovo Cimento B **46**, 145 (1966).
[18]J. C. Camparo and R. P. Frueholz, J. Appl. Phys. **59**, 301 (1986).
[19]J. C. Camparo and R. P. Frueholz, J. Appl. Phys. **59**, 3313 (1986).
[20]J. C. Camparo and R. P. Frueholz, IEEE Trans. Ultrasonic. Ferroelec. Freq. Control **UFFC-34**, 607 (1987).
[21]J. C. Camparo and R. P. Frueholz, IEEE Trans. Ultrasonic. Ferroelec. Freq. Control (to be published).
[22]As discussed in Ref. 11 the saturated linewidths in this multilevel system will in general be larger than the Rabi frequency. However, the scaling factor is a constant, and does not affect the functional relationship between the saturated linewidth and the magnitude of the saturating field strength.
[23]For a discussion of the laws of Bouger, Lambert, and Beer and how they differ see J. H. Goldstein and R. A. Day, J. Chem. Educ. **31**, 417 (1954); D. F. Swinehart, *ibid.* **39**, 333 (1962), and references therein.
[24]J. C. Camparo, R. P. Frueholz, and C. H. Volk, Phys. Rev. A **27**, 1914 (1983).
[25]J. C. Camparo, R. P. Frueholz, and C. M. Klimcak, Phys. Rev. A **36**, 2072 (1987).
[26]S. L. Chin and N. R. Isenor, Can. J. Phys. **48**, 1445 (1970).
[27]P. Lambropoulos, Phys. Lett. **40A**, 199 (1972).